Galactic kinematics and dynamics from Radial Velocity Experiment stars

J. Binney,[1]⋆ B. Burnett,[1] G. Kordopatis,[2] M. Steinmetz,[3] G. Gilmore,[2] O. Bienayme,[4] J. Bland-Hawthorn,[5] B. Famaey,[4] E. K. Grebel,[6] A. Helmi,[7] J. Navarro,[8]† Q. Parker,[9,10] W. A. Reid,[9] G. Seabroke,[11] A. Siebert,[4] F. Watson,[10] M. E. K. Williams,[3] R. F. G. Wyse[12] and T. Zwitter[13,14]

[1]*Rudolf Peierls Centre for Theoretical Physics, Keble Road, Oxford OX1 3NP, UK*
[2]*Institute of Astronomy, Madingley Road, Cambridge CB3 0HA, UK*
[3]*Leibniz-Institut für Astrophysik Potsdam (AIP), An der Sternwarte 16, D-14482 Potsdam, Germany*
[4]*Observatoire Astronomique de Strasbourg, 11 rue de l'Université, F-67000 Strasbourg, France*
[5]*Sydney Institute for Astronomy, School of Physics A28, University of Sydney, NSW 2006, Australia*
[6]*Astronomisches Rechen-Institut, Zentrum für Astronomie der Universität Heidelberg, Mönchhofstr 12-14, D-69120 Heidelberg, Germany*
[7]*Kapteyn Astronomical Institute, University of Groningen, Landleven 12, NL-9747 AD Groningen, the Netherlands*
[8]*University of Victoria, BC V8P 5C2, Canada*
[9]*Macquarie University, Balalava Road, NSW 2109, Australia*
[10]*Australian Astronomical Observatory, PO Box 915, North Ryde, NSW 1670, Australia*
[11]*Mullard Space Science Laboratory, University College London, Holmbury St Mary, Dorking RH5 6NT, UK*
[12]*Department of Physics and Astronomy, Johns Hopkins University, 366 Bloomberg center, 3400 N. Charles St, Baltimore, MD 21218, USA*
[13]*Faculty of Mathematics and Physics, University of Ljubljana, Jadranska 19, 1000 Ljubljana, Slovenia*
[14]*Center of Excellence SPACE-SI, Aškerčeva cesta 12, 1000 Ljubljana, Slovenia*

ABSTRACT

We analyse the kinematics of $\sim$400 000 stars that lie within $\sim$2 kpc of the Sun and have spectra measured in the Radial Velocity Experiment. We decompose the sample into hot and cold dwarfs, red-clump and non-clump giants. The kinematics of the clump giants are consistent with being identical with those of the giants as a whole. Without binning the data we fit Gaussian velocity ellipsoids to the meridional-plane components of velocity of each star class and give formulae from which the shape and orientation of the velocity ellipsoid can be determined at any location. The data are consistent with the giants and the cool dwarfs sharing the same velocity ellipsoids, which have vertical velocity dispersion rising from 21 km s^{-1} in the plane to $\sim$55 km s^{-1} at $|z| = 2$ kpc and radial velocity dispersion rising from 37 km s^{-1} to 82 km s^{-1} in the same interval. At (R, z), the longest axis of one of these velocity ellipsoids is inclined to the Galactic plane by an angle $\sim$0.8 arctan(z/R). We use a novel formula to obtain precise fits to the highly non-Gaussian distributions of v_ϕ components in eight bins in the (R, z) plane. We compare the observed velocity distributions with the predictions of a published dynamical model fitted to the velocities of stars that lie within $\sim$150 pc of the Sun and star counts towards the Galactic pole. The predictions for the v_z distributions are exceptionally successful. The model's predictions for v_ϕ are successful except for the hot dwarfs, and its predictions for v_r fail significantly only for giants that lie far from the plane. If distances to the model's stars are overestimated by 20 per cent, the predicted distributions of v_r and v_z components become skew, and far from the plane broader. The broadening significantly improves the fits to the data. The ability of the dynamical model to give such a good account of a large body of data to which it was not fitted inspires confidence in the fundamental correctness of the assumed, disc-dominated, gravitational potential.

Key words: Galaxy: disc – solar neighbourhood – galaxies: kinematics and dynamics.

⋆ E-mail: binney@thphys.ox.ac.uk
† Senior ClfAR Fellow.

1 INTRODUCTION

A major strand of contemporary astronomy is the quest for an understanding of how galaxies formed and evolved within the context of the concordance cosmological model, in which the cosmic energy density is dominated by vacuum energy and the matter density is dominated by some initially cold matter that does not interact electromagnetically. This quest is being pursued on three fronts: observations of objects seen at high redshifts and early times, simulations of clustering matter and star formation, and by detailed observation of the interplay between the chemistry and dynamics of stars in our own Galaxy.

As a contribution to this last 'Galactic archaeology' strand of the quest for cosmic understanding, the Radial Velocity Experiment (RAVE; Steinmetz et al. 2006) has since 2003 gathered spectra at resolution ~7500 around the Ca II near-IR triplet of ~400 000 stars. The catalogued stars are roughly half giants and half dwarfs, and mostly lie within 2.5 kpc of the Sun (Burnett et al. 2011; Binney et al. 2013). The RAVE survey is complementary to the Sloan Digital Sky Survey (SDSS; York et al. 2000) and the latter's continuations (Yanny et al. 2009; Eisenstein et al. 2011) in that it observes stars at least as bright as $I = 9$–13, whereas the SDSS observes stars fainter than $g = 14$. On account of the faint magnitudes of the SDSS stars, they are overwhelmingly at distances greater than 0.5 kpc so the Galaxy's thin disc, which has a scaleheight ~0.3 kpc and is by far the dominant stellar component of the Galaxy, contributes a small proportion of the stars in the SDSS data releases. The thin and thick discs, by contrast, completely dominate the RAVE catalogue.

Recently, Binney et al. (2013) derived distances to ~400 000 stars from 2MASS photometry and the stellar parameters produced by the VDR4 spectral-analysis pipeline described by Kordopatis et al. (2013). We use these distances to discuss the kinematics of the Galaxy in the extended solar neighbourhood, that is, in the region within ~2 kpc of the Sun. Since the selection criteria of the RAVE survey are entirely photometric, we can determine the distribution of the velocities of survey stars within the surveyed region without determining the survey's complete selection function, which is difficult (see Piffl & Steinmetz in preparation; Sharma et al., in preparation).

We characterize the kinematics in several distinct ways. In Section 3, we obtain analytic fits to the variation within the (R, z) plane of the velocity ellipsoid by a technique that avoids binning stars (Burnett 2010). In Section 4, we bin stars to obtain histograms of the distribution of three orthogonal components of velocity. We use a novel formalism to obtain analytic fits to the distributions of the azimuthal component of velocity. We examine the first and second moments of the distributions of the velocity components parallel to the principal axes of the local velocity ellipsoid. The second moments are consistent with our previously derived values, but some first moments are non-zero: values ~1.5 km s^{-1} are common and values as large as 5 km s^{-1} occur.

In Section 5, we compare our results with the predictions of a dynamical model Galaxy that is based on Jeans' theorem. Although this model, which was described by Binney (2012; hereafter B12), was not fitted to any RAVE data, we find that its predictions for the distributions of vertical components are extremely successful, while those for the radial components are successful at $|z| < 0.5$ kpc but become less successful further from the plane, where they produce velocity distributions that are too narrow and sharply peaked. In Section 5.3, we investigate the impact of systematically overestimating distances to stars. When distances to the model's stars are overestimated by 20 per cent, the predicted distributions of v_r and v_z acquire asymmetries that are similar to those sometimes seen in the data. Systematic overestimation of distances brings the model into better agreement with data far from the plane by broadening its v_r distributions.

2 INPUT PARAMETERS AND DATA

Throughout this paper, we adopt $R_0 = 8$ kpc as the distance of the Sun from the Galactic Centre, $\Theta_0 = 220$ km s^{-1} for the local circular speed and from Schönrich, Binney & Dehnen (2010) $(U_0, V_0, W_0) = (11.1, 12.24, 7.25)$ km s^{-1} as the velocity of the Sun with respect to the local standard of rest. While our values of R_0 and Θ_0 may be smaller than they should be (e.g. McMillan 2011), we adopt these values in order to be consistent with the assumptions inherent in the B12 model.

Proper motions for RAVE stars can be drawn from several catalogues. Williams et al. (2013) compare results obtained with different proper-motion catalogues, and on the basis of this discussion, we originally decided to work with the PPMX proper motions (Röser et al. 2008) because these are available for all our stars and they tend to minimize anomalous streaming motions. However, when stars are binned spatially and one computes the dispersions in each bin of the raw velocities $4.73\mu(s/\text{kpc}) + v_{\text{los}}$ from the PPMX proper motions, the resulting dispersions for bins at distances $\gtrsim 0.5$ kpc are often smaller than the contributions to these from proper-motion errors alone. It follows that either our distances are much too large or the quoted proper-motion errors are seriously overestimating the true random errors. The problem can be ameliorated by cutting the sample to exclude stars with large proper-motion errors, but there are still signs that the velocity dispersions in distant bins are coming out too small on account of an excessive allowance for the errors in the proper motions of stars that have small proper motions. The errors in the UCAC4 catalogue (Zacharias et al. 2013) are ~60 per cent of those in the PPMX catalogue, and the problem just described does not arise with these proper motions, so we have used them. We do, however, exclude stars with an error in μ_b greater than 8 mas yr^{-1}.

In addition to this cut on proper-motion error, the sample is restricted to stars for which Binney et al. (2013) determined a probability density function (PDF) in distance modulus. To belong to this group a star has to have a spectrum that passed the Kordopatis et al. (2013) pipeline with signal-to-noise ratio of 10 or more.

3 FITTING MERIDIONAL COMPONENTS WITHOUT BINNING THE DATA

At each point in the Galaxy a stellar population that is in statistical equilibrium in an axisymmetric gravitational potential $\Phi(R, z)$ should define a velocity ellipsoid. Two of the principal axes of this ellipsoid should lie within the (R, z) plane, with the third axis in the azimuthal direction e_ϕ. Near the plane the ellipsoid's longest axis is expected to point roughly radially and the shortest axis vertically. Let e_1 be the unit vector along the longest axis and e_3 be the complementary unit vector, and let $\theta(R, z)$ denote the angle between e_1 and the Galactic plane.

The lengths of the principal semi-axes of the velocity ellipsoid are of course the principal velocity dispersions

$$\sigma_1(R, z) = \langle (\boldsymbol{v} \cdot \boldsymbol{e}_1)^2 \rangle^{1/2}$$

$$\sigma_\phi(R, z) = (\langle (\boldsymbol{v} \cdot \boldsymbol{e}_\phi)^2 \rangle - \langle \boldsymbol{v} \cdot \boldsymbol{e}_\phi \rangle^2)^{1/2}$$

$$\sigma_3(R, z) = \langle (\boldsymbol{v} \cdot \boldsymbol{e}_3)^2 \rangle^{1/2}. \tag{1}$$

Table 1. Test of the fitting procedure. The bottom row gives the parameters used to choose the velocities, while top row gives the values of the parameters in equation (4) from which FRPRMN started. The second row shows the values of the parameters on which it converged given data at the locations of the 40 175 clump giants. The third, fourth and fifth rows give the parameters values similarly obtained using data at the locations of 181 725 non-clump giants, 55 398 hot dwarfs and 95 470 cool dwarfs, respectively.

	a_0	a_1	a_2	a_3	a_4	a_5	a_6	a_7	a_8
Start	1	0.5	0.1	2	1	1	0.2	5	1
Clump giants	0.506	1.011	0.414	5.355	0.549	0.493	0.307	11.425	0.433
Non-clump giants	0.491	0.998	0.482	6.519	0.462	0.499	0.347	9.768	0.511
Hot dwarfs	0.459	0.994	0.611	3.329	2.194	0.499	0.448	5.241	1.598
Cool dwarf	0.587	1.003	0.541	2.905	1.841	0.499	0.210	5.505	1.500
Truth	0.5	1	0.4	6	0.5	0.5	0.4	10	0.5

In the following we shall use the notation

$$V_1 \equiv \mathbf{v} \cdot \mathbf{e}_1 \text{ and } V_3 \equiv \mathbf{v} \cdot \mathbf{e}_3. \qquad (2)$$

We estimate the functional forms of σ_1 and σ_3 as follows.

We let $\theta(R, z)$ be determined by a single parameter a_0 through

$$\theta = a_0 \arctan(z/R). \qquad (3)$$

We use four further parameters a_i to constrain the behaviour of σ_1, and similarly for σ_3, by writing

$$\sigma_1(R, z) = \sigma_0 a_1 \exp[-a_2(R/R_0 - 1)][1 + (a_3 z/R)^2]^{a_4}$$
$$\sigma_3(R, z) = \sigma_0 a_5 \exp[-a_6(R/R_0 - 1)][1 + (a_7 z/R)^2]^{a_8}, \qquad (4)$$

where $\sigma_0 \equiv 30 \text{ km s}^{-1}$ ensures that all the a_i are dimensionless and of order unity. These forms are the fruit of a combination of physical intuition and some experimentation. In particular, by symmetry we require even functions of z that have vanishing vertical gradients in the plane, and experimentation shows that power series in z^2 do not work well. Secondly, it has been conventional to assume exponential dependence of velocity dispersion on R since the scaleheights of discs were found to be roughly constant (van der Kruit & Searle 1981). Moreover, the data cover a significant range in R only at large $|z|$, so we are not in a position to consider elaborate dependence on R. The parameters a_1 and a_5 set the overall velocity scale of σ_1 and σ_3, respectively, while a_2 and a_6 determine how fast these dispersions decrease with increasing radius. The parameter pairs (a_3, a_4) and (a_7, a_8) determine how the dispersions vary with distance from the plane.

From equations (4), it is straightforward to calculate the derivatives with respect to the nine parameters a_i of the components V_1 and V_3 of a star's velocity and of the dispersions σ_i, so we use a conjugate-gradient method to extremize the log likelihood,

$$\sum_{\text{stars}} \sum_{i=1,3} \ln[\sigma_i^2 + e^2(V_i)] + \frac{V_i^2}{\sigma_i^2 + e^2(V_i)}, \qquad (5)$$

associated with a correctly normalized biaxial Gaussian PDF in (V_1, V_2) space. Here, $e(V_i)$ is the formal error in V_i for a given star. This is computed from the quoted errors on the proper motions and the line-of-sight velocity assuming the distance to be inverse of the expectation of the parallax given by Binney et al. (2013), who found this to be the most reliable distance estimator. With the present method it is exceedingly hard to allow for distance errors, and we do not do this.

The code for extracting the values of the a_i from a catalogue of stellar phase-space coordinates was tested as follows. The velocity of each RAVE star was replaced by a velocity chosen at random from a triaxial Gaussian velocity distribution with variances $\sigma_i^2(R, z) + e^2(V_i)$, where the σ_i were derived from plausible values of the

a_i and the errors $e(V_i)$ are the actual errors on that star's velocity components. Then the routine FRPRMN of Press et al. (1994) was used to maximize the function (5) starting from another set of values of the a_i. The conventional χ^2 is

$$\chi^2 = \sum_{\text{stars}} \sum_{i=1,3} \frac{V_i^2}{\sigma_i^2 + e^2(V_i)}. \qquad (6)$$

In all tests the chosen model yielded a value of χ^2 per degree of freedom that differed from unity by less than 3×10^{-4}.

We have analysed separately four classes of stars: clump giants ($0.55 \leq J - K \leq 0.8$ and $1.7 \leq \log g < 2.4$), non-clump giants ($\log g < 3.5$), hot ($T_{\text{eff}} > 6000$ K) dwarfs and cool dwarfs.

The first row of Table 1 shows the parameters from which fitting started, while the bottom row gives the values of the parameters that were used to assign velocities to the stars. The second row shows the parameter values upon which FRPRMN converged with data at the locations of 40 175 red-clump stars in the RAVE sample. The third row gives the results obtained using the sample's 181 726 non-clump giants. The fourth and fifth rows give, respectively, results obtained using the 55 398 hot dwarfs and 95 469 cool dwarfs.

Naturally, the precision with which the parameters can be recovered from the data increases with the size and spatial coverage of the sample. Hence, the cold dwarfs deliver the least, and the giants the most, accurate results. The parameters that are most accurately recovered are a_1 and a_5, which control the magnitudes of dispersions, and a_0, which controls the tilt of the velocity ellipsoid. The parameters a_3 and a_4, which control the vertical variation of the radial dispersion, and a_7 and a_8, which control the vertical variation of the vertical dispersion, are recovered quite well from the giants but rather poorly from the dwarfs. However, even the dwarfs yield quite accurate values for the products $a_3^2 a_4$ and $a_7^2 a_8$ that occur in the first non-trivial term in the Maclaurin series of the final brackets of equations (4). The parameters a_2 and a_6, which control radial gradients are recovered only moderately well by all star classes.

When fitting the measured velocities of RAVE stars, the difference between unity and χ^2 per degree of freedom for the chosen model ranged from 3.5×10^{-3} for cold dwarfs to 1.7×10^{-2} for non-clump giants. Table 2 shows the parameters of the chosen models. Both classes of giants and the cool dwarfs yield similar values $a_0 \simeq 0.8$ of the parameter that controls the orientation of the velocity ellipsoid. Since this value lies close to unity, the long axis of the velocity ellipsoid points almost to the Galactic Centre (Fig. 1) consistent with the findings of Siebert et al. (2008). The hot dwarfs yield a much smaller value, $a_0 \simeq 0.2$, so the long axis of their velocity ellipsoid does not tip strongly as one moves up.

The velocity dispersions in the plane are $\sigma_R = 30 a_1 \text{ km s}^{-1}$ and $\sigma_z = 30 a_5 \text{ km s}^{-1}$. The smallest dispersions, $(\sigma_R, \sigma_z) = (29.3, 14.0)$,

Table 2. Velocity ellipsoids from measured velocities. When the values given here are inserted into equations (3) and (4), one obtains expressions for the semi-axis lengths and orientation of the velocity ellipsoids at a general point (R, z). From top to bottom the rows give results for clump giants, non-clump giants, and hot and cool dwarfs.

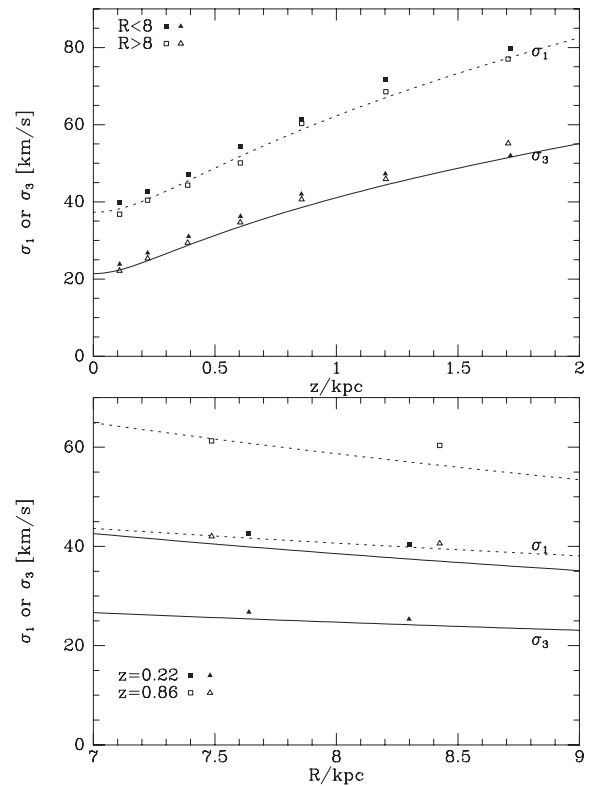|	a_0	a_1	a_2	a_3	a_4	a_5	a_6	a_7	a_8
Clump giants	0.872	1.183	0.394	24.835	0.212	0.682	0.554	29.572	0.211
Non-clump giants	0.815	1.243	0.398	25.283	0.214	0.713	0.362	34.815	0.218
Hot dwarfs	0.213	0.976	0.719	7.891	1.282	0.468	−0.209	26.992	0.380
Cool dwarfs	0.815	1.153	1.142	47.112	0.169	0.711	1.572	9.852	1.200
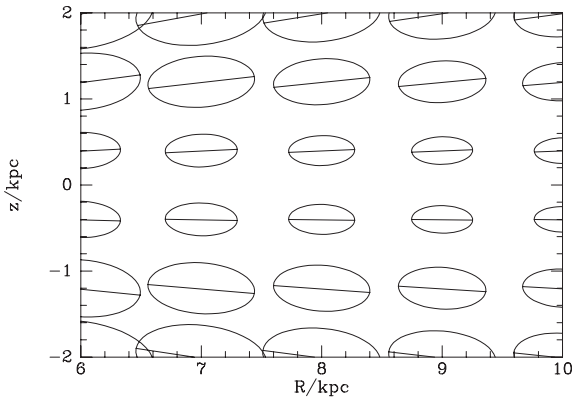
Figure 1. Representation of the velocity ellipsoids of giant stars; the lengths of the principal axes of each ellipse are proportional to the corresponding velocity dispersion at the centre of the ellipse.

Figure 2. The curves show the spatial variation of the values of σ_3 and σ_1 at fixed R (top) or z (below) that are extracted from the raw data for non-clump giant stars by a maximum-likelihood technique that takes into account random measuring errors. The black dots show the result of correcting the dispersions of binned data for measurement errors by simple quadrature subtraction. In the upper panel, the upper point of each pair refers to a bin that lies inside R_0 and the lower point refers to a bin at $R > R_0$. In the lower panel, results are shown for $z = 0.22$ and 0.86 kpc.

are for the hot dwarfs and the largest, (37.3, 21.4), are for the giants. For the giants and cool dwarfs, we have $\sigma_z/\sigma_R = a_5/a_1 \simeq 0.6$, while for the hot dwarfs, we have $\sigma_z/\sigma_R \simeq 0.48$, significantly smaller.

The scalelengths on which the dispersions vary are $R_\sigma = R_0/a_2$ for σ_r and $R_\sigma = R_0/a_6$ for σ_z. For the giants these are $\sim 2.5R_0$, which is surprisingly large: one anticipates $R_\sigma \lesssim 3R_d \simeq R_0$. The cool dwarfs, by contrast yield $R_\sigma < R_0$. For σ_r, the hot dwarfs yield $R_\sigma \simeq 1.4R_0$, but for σ_z they yield a negative value of R_σ, implying that σ_z *increases* with radius. Given that the survey volume is a cone that excludes the plane, not only is it hard to disentangle radial and vertical gradients, but stars such as hot dwarfs that are strongly concentrated to the plane do not probe a large volume and consequently are not suited to measuring gradients. Moreover, the longest axis of the velocity ellipsoids of populations of young stars are known not to lie within the (R, z) plane – the 'vertex deviation' (e.g. Dehnen & Binney 1998). This phenomenon is evidence that these populations are not in dynamical equilibrium as our methodology assumes, either because they are too young or because they are strongly disturbed by spiral structure.

The upper panel of Fig. 2 shows the dependences on z at $R = 8$ kpc of σ_1 (dashed line) and σ_3 (full line) that are implied by Table 2 for non-clump giants. The squares and triangles show velocity dispersions estimated by binning the data as described in Section 4 below. The lower panel shows the corresponding radial dependences at $z = 0.22$ and 0.86 kpc.

In Fig. 3, the full black curves show the runs with z at $R = R_0$ of σ_1 and σ_3 for non-clump giants, while the dashed red curves show the same quantities for the cool dwarfs. From these plots, we infer that the dispersions of the cool dwarfs are probably consistent with those for non-clump giants except very near the plane where σ_1 may be lower for the dwarfs. The blue dotted curves show the distinctly lower velocity dispersions of the hot dwarfs: lower

dispersions are to be expected of such relatively young stars since they have experienced less stochastic acceleration than older stars.

4 USING BINNED DATA

4.1 Azimuthal velocities

In a disc galaxy, the distribution of v_ϕ components is inherently skew and the skewness of the distribution contains essential information about the system's history and dynamics. Consequently, it is not appropriate to use the machinery described in the last section to fit observed v_ϕ distributions.
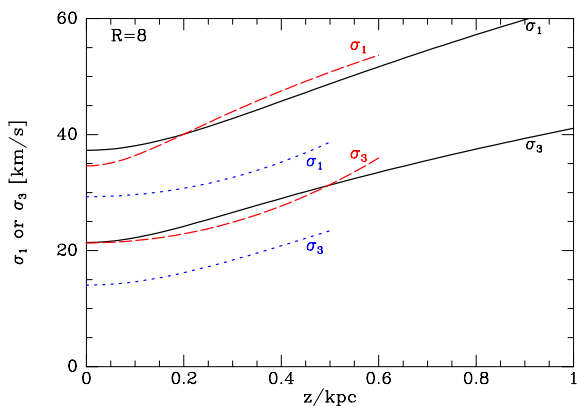
Figure 3. The dependence on $|z|$ of the velocity dispersions at R_0. The full black curves are for non-clump giants, red dashed curves are for cool dwarfs and dotted blue curves are for hot dwarfs.

The v_ϕ distributions of the dynamical models described by B12, which will be discussed in Section 5 below, can be fitted extremely well by the following analytic distribution

$$P(v_\phi) = \text{constant} \times e^{-(v_\phi - b_0)^2/2\sigma_\phi^2}, \tag{7}$$

where σ_ϕ is a cubic in v_ϕ:

$$\sigma_\phi(v_\phi) = b_1 + b_2 v_{\phi 100} + b_3 v_{\phi 100}^2 + b_4 v_{\phi 100}^3, \tag{8}$$

with $v_{\phi 100} \equiv v_\phi/100 \,\text{km s}^{-1}$. The general idea here is that b_0 defines a characteristic streaming velocity, while b_1 is a basic azimuthal velocity dispersion. The parameters b_2–b_4 cause the velocity dispersion σ_ϕ to increase/decrease as v_ϕ moves below/above the circular speed, thus making the v_ϕ distribution skew.

In principle, functional forms could be adopted for the dependence on (R, z) of the parameters b_i appearing in equations (7) and (8), and then, in strict analogy to the work of the previous section, the values of the parameters appearing in these functional forms could be determined by maximizing the likelihood of the data given distribution (7). Unfortunately, for this scheme to be viable, we require an expression for the value of the normalizing constant as a function of the parameters, and no such formula is available. Therefore, we have determined the b_i by binning the data and performing a least-squares fit of equation (7) convolved with the observational errors to the histogram of the binned data.

The stars were divided into eight spatial bins according to whether $R < R_0$ or $R > R_0$ and $|z|$ lay in intervals bounded by (0, 0.3, 0.6, 1, 1.5) kpc for giants or (0, 0.15, 0.3, 0.45, 0.6) kpc for dwarfs. Table 3 gives the parameters that fit the v_ϕ distributions of the clump stars (upper block) and non-clump giants (lower block). Table 4 gives values of the parameters for the hot (upper block) and cool dwarfs. The black points in Figs 4–7 show the observational histograms. At the top left of each panel, we give the mean values of $(R, |z|)$ and $e(v_\phi)$ for stars in the bin, where the latter is the rms error for the stars in the given bin. Also, given at the top of each panel is the mean velocity, $\langle v_\phi \rangle$, which of course is sensitive to our adopted values $\Theta_0 = 220 \,\text{km s}^{-1}$ and $v_{\phi\odot} = \Theta_0 + 12.24 \,\text{km s}^{-1}$. The values of $\langle v_\phi \rangle$ are also given in Tables 3 and 4, where we see that on account of the skewness of the v_ϕ distributions, $\langle v_\phi \rangle$ is systematically smaller than the fit parameter b_0, which would be the mean velocity if σ_ϕ were not a function of v_ϕ.

In Figs 4–7, bins with $R < R_0$ are shown in the left-hand column, bins with $R > R_0$ are shown in the right-hand column and $|z|$ increases downwards. The dotted curves show the functions defined

Table 3. Values of the mean streaming velocity and the parameters defined by equations (7) and (8) required to fit the v_ϕ distributions of RAVE stars. The upper block refers to red clump stars and the lower one to non-clump giants.

$(R, |z|)$	$\overline{v}_\phi$	b_0	b_1	b_2	b_3	b_4
(7.61, 0.19)	217.9	224.2	51.0	−5.79	−9.78	2.81
(8.36, 0.19)	211.4	215.5	45.1	−2.48	−12.34	3.60
(7.51, 0.44)	210.8	222.0	58.6	−14.91	0.07	0.20
(8.36, 0.43)	207.9	214.7	49.7	−2.70	−12.22	3.43
(7.48, 0.75)	199.0	207.3	71.2	−50.09	27.76	−5.55
(8.41, 0.75)	200.1	211.4	62.4	−18.73	−0.20	0.63
(7.52, 1.18)	189.3	195.8	71.2	−39.27	18.50	−3.27
(8.37, 1.19)	191.2	201.9	70.1	−30.49	9.61	−1.44
(7.66, 0.19)	215.6	223.3	53.6	−4.15	−12.21	3.36
(8.28, 0.19)	209.8	215.1	52.8	−11.90	−7.53	2.74
(7.54, 0.43)	208.7	219.2	63.8	−21.69	1.61	0.31
(8.34, 0.42)	206.4	213.5	57.0	−12.40	−7.85	2.83
(7.48, 0.75)	198.2	206.7	72.0	−41.92	17.72	−2.96
(8.42, 0.75)	198.7	209.3	66.1	−23.36	1.59	0.53
(7.50, 1.20)	186.6	193.3	76.4	−42.35	16.29	−2.28
(8.42, 1.20)	190.2	200.3	78.0	−44.79	18.81	−3.20

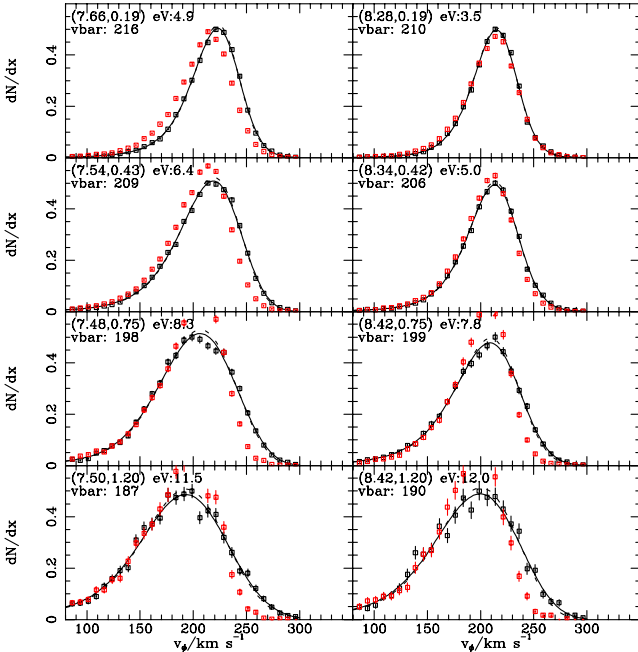**Table 4.** The same as Table 3, but for hot (upper block) and cool (lower block) dwarfs.

$(R, |z|)$	$\overline{v}_\phi$	b_0	b_1	b_2	b_3	b_4
(7.85, 0.10)	220.1	224.9	69.5	−44.33	10.68	−0.73
(8.11, 0.11)	216.5	220.1	29.3	20.80	−24.86	5.67
(7.80, 0.22)	220.7	224.4	29.8	20.98	−24.10	5.36
(8.13, 0.22)	217.5	221.3	29.6	21.56	−25.23	5.69
(7.78, 0.36)	219.5	225.0	46.9	−0.85	−13.53	3.59
(8.15, 0.36)	215.8	219.2	79.2	−56.54	14.43	−0.71
(7.79, 0.50)	217.6	223.2	46.8	−3.40	−10.04	2.75
(8.15, 0.50)	214.3	218.7	69.6	−37.94	5.23	0.74
(7.90, 0.09)	215.8	222.2	−9.6	98.37	−66.58	12.49
(8.06, 0.08)	213.7	219.9	−18.9	111.09	−72.53	13.42
(7.84, 0.21)	211.1	219.7	18.8	52.04	−41.09	8.08
(8.10, 0.21)	211.1	217.6	−4.6	87.28	−59.59	11.26
(7.81, 0.36)	211.5	219.9	19.7	58.80	−47.62	9.56
(8.12, 0.35)	207.7	215.2	57.3	−12.98	−8.21	2.90
(7.73, 0.50)	203.6	216.1	22.4	52.28	−39.99	7.54
(8.16, 0.51)	210.9	218.4	8.8	87.40	−67.29	13.41

by the b_i in Tables 3 and 4, while the full curves show the results of convolving these curves with the Gaussian of dispersion $e(v_\phi)$. The dotted curves are mostly obscured by the full curves because observational errors do not have a big impact on these data. All histograms are fitted to great precision by the full curves.

Figs 8 and 9 show, respectively, the mean rotation velocity of the giants and dwarfs as functions of distance from the plane. The data points were obtained by fitting the analytic model convolved with the measurement errors to histograms of v_ϕ components with the stars placed in seven bins at each of $R < R_0$ and $R > R_0$, and then calculating for each bin the mean velocity of the model distribution before convolution by error. We do not show error bars, but the statistical errors on these points are very small. All these points would move upwards by $20 \,\text{km s}^{-1}$, if we increased our estimate of the local circular speed from $\Theta_0 = 220$ to $= 240 \,\text{km s}^{-1}$, and they would move down by $5 \,\text{km s}^{-1}$, if we decreased our estimate of $v_{\phi\odot} - \Theta_0$ from 12.24 to $7.24 \,\text{km s}^{-1}$. In Fig. 8, the points for giants show a clear trend for $\langle v_\phi \rangle$ to decline with distance from
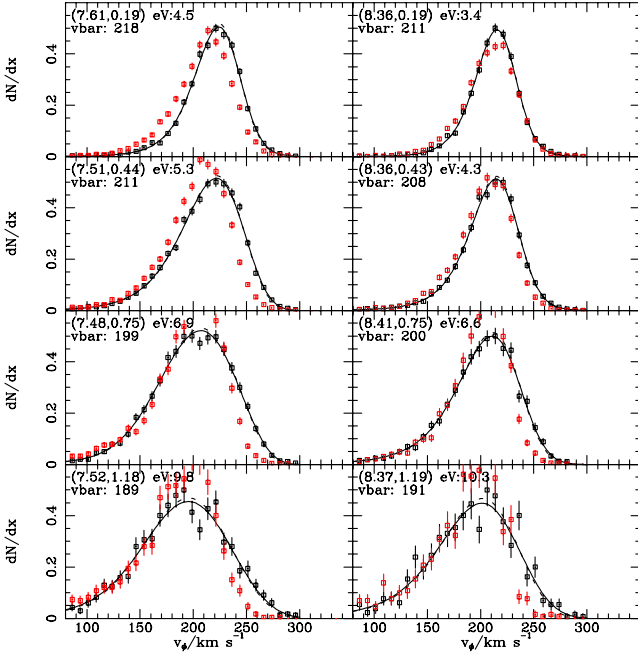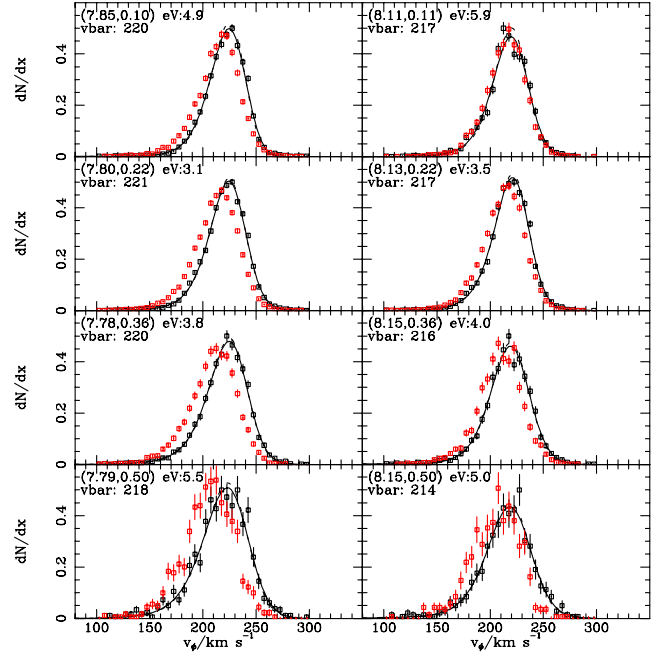
Figure 4. The distributions of v_ϕ for red-clump giants (black data points) and fits to them – in each panel the dashed curve shows the kinematic model specified by equations (7) and (8), while the full curve shows the model convolved with the mean errors in v_ϕ. The red points show the predictions of the B12 dynamical model. The mean coordinates of the stars in each bin are given at top left, followed by the rms velocity error (eV) and the sample mean of v_ϕ (vbar). In this and all subsequent histograms, the horizontal bars span the width of the bins and the vertical bars indicate Poisson errors.

Figure 6. As Fig. 4, but for hot dwarfs.

Figure 5. As Fig. 4, but for non-clump giant stars.
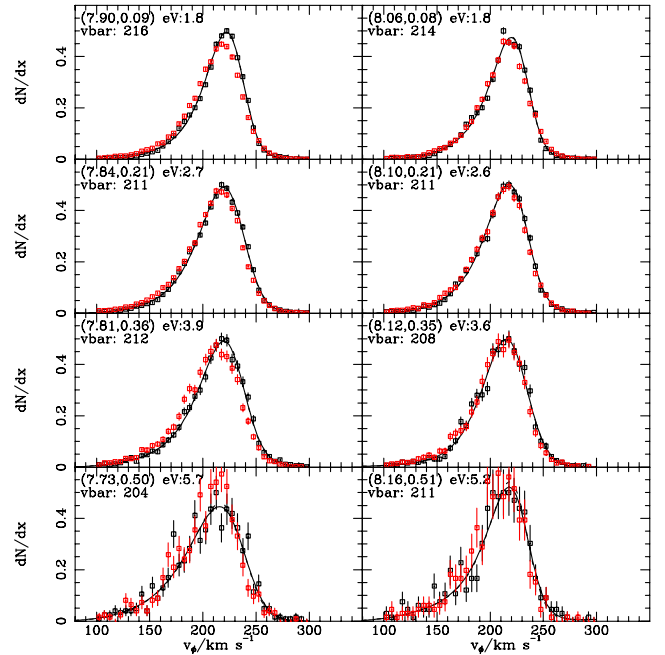
Figure 7. As Fig. 4, but for cool dwarfs.

the plane, as we expect given that along this sequence σ_1 rises and increases the asymmetric drift $v_a \sim \sigma_1^2/v_c$.

In Fig. 9, the point for hot dwarfs at $z \lesssim 50\,\mathrm{pc}$ and $R < R_0$ is $\sim25\,\mathrm{km\,s^{-1}}$ larger than the corresponding point at $R > R_0$, so both points are highly anomalous. However, the histograms for the

associated bins (which we do not show) indicate that the anomaly is not caused by small-number statistics. The points for larger distances from the plane lie close to the circular speed at $R < R_0$ and fall about $4\,\mathrm{km\,s^{-1}}$ lower at $R > R_0$. These differences could well reflect spiral structure. The points for cool dwarfs show a slight fall with increasing distance from the plane and a tendency to be up to $2\,\mathrm{km\,s^{-1}}$ lower at $R > R_0$ than at $R < R_0$. The fall in $\langle v_\phi \rangle$ between the plane and 0.5 kpc is consistent with that of the giants.
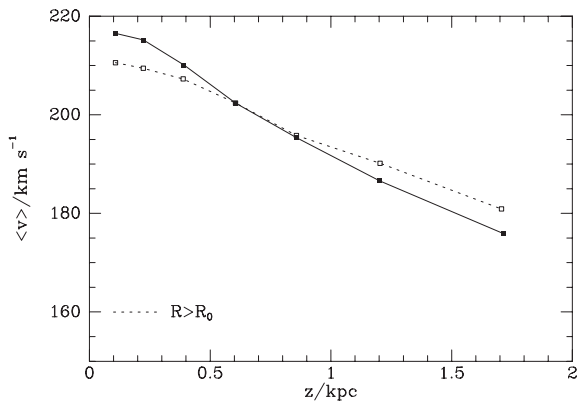
Figure 8. The mean rotation velocity of the giants as a function of distance from the plane. The full curve is for bins at $R < R_0$. The data points are for the means of model distributions like those plotted as dotted curves in Fig. 5. The statistical errors on these points are very small.
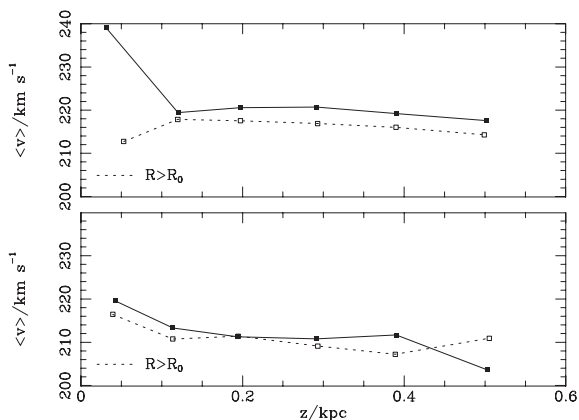

Figure 9. As Fig. 8, but for the dwarfs: hot (top) and cool (below).

4.2 Moments of the V_1 and V_3 distributions

The black points in Figs 11–14 show, for hot dwarfs, cool dwarfs, clump and non-clump giants respectively, the distributions of the meridional-plane components V_1 and V_3 defined by equations (2). At the bottom centre of each panel, the numbers in brackets give the mean values of R and $|z|$ for the stars in each bin, the standard deviation of the data (sD), the value at this location of the relevant velocity dispersion from the Gaussian model of Section 3 (sM), the mean velocity of the stars in the bin (mV) and the rms measurement error for those stars (eV). The agreement between the standard deviations of the data and the model dispersion at the bin's barycentre is typically excellent.

If the Galaxy were in an axisymmetric equilibrium and we were using the correct value for the Sun's peculiar velocity, the mean velocities would all vanish to within the discreteness noise, but they do not. All the three older populations show similar trends in mean velocities: the means of V_3 tend to be negative at $R > R_0$ and increase in absolute value away from the plane, while the mean values of V_1 fall from positive to negative as one moves away from the plane with the largest absolute values occurring for giants near the plane. Siebert et al. (2011) and Williams et al. (2013) have analysed similar statistically significant mean velocities in velocities of RAVE stars drawn from an earlier spectral-analysis pipeline than that used here. We defer discussion of this phenomenon until Section 5.3.
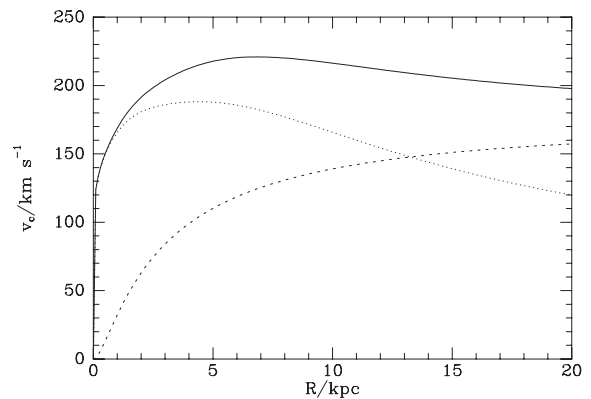

Figure 10. Dotted curve: the contribution to the circular speed from the disc and bulge components; dashed curve: the contribution of the dark halo.

5 COMPARISONS WITH DYNAMICAL MODELS

It is interesting to compare the observed distributions with ones predicted by the favoured equilibrium dynamical model of B12. This model is defined by a gravitational potential and a DF. The potential is generated by thin and thick exponential stellar discs, a gas layer, a flattened bulge and a dark halo. Fig. 10 shows the contributions to the circular speed from the baryons (dotted curve) and from the dark halo (dashed curve). One sees that this is a maximum-disc model. In fact, 65 per cent of the gravitational force on the Sun is produced by baryons rather than dark matter.

The distribution function (DF) is an analytic function $f(\mathbf{J})$ of the three action integrals J_i. The function, which specifies the density of stars in three-dimensional action space, has nine parameters. Four parameters specify each of the thin and thick discs and one parameter specifies the relative weight of the thick disc. Their values are given in column (b) of table 2 in B12. They were chosen by fitting the model's predictions for the velocity distribution of solar-neighbourhood stars to that measured by the Geneva–Copenhagen survey (GCS) of F and G stars (Holmberg, Nordström & Andersen 2007), and to the vertical density profile of the disc determined by Gilmore & Reid (1983). Hence, the data to which this DF was fitted do not include velocities in the region distance $s \gtrsim 150\,\mathrm{pc}$ within which most RAVE stars lie, and whatever success the DF has in *predicting* the velocities of RAVE stars must be considered a non-trivial support for the assumptions that went into the model, which include the use of a particular, disc-dominated, gravitational potential and the functional form of the DF.

We have used the B12 DF to generate pseudo-data for each star in the RAVE sample from the model's velocity distribution as follows. We start by choosing a possible true location $\mathbf{x}'$ by picking a distance s' from the multi-Gaussian model of the star PDF in distance s that Binney et al. (2013) produced. We then sample the velocity distribution of the dynamical model for that class of star at $\mathbf{x}'$ and compute the corresponding proper motions and line-of-sight velocity v_{los}. To these observables, we add random errors drawn from the star's catalogued error distributions and from the modified observables compute the space velocity using the catalogued distance s rather than the hypothesized true distance s'. This procedure comes very close to reproducing the data that would arise if the Galaxy were correctly described by the model, each star's distance PDF were sound and the errors on the velocities had been correctly assessed: it does not quite achieve this goal on account of a subtle effect, which is costly to allow for. This effect causes the procedure
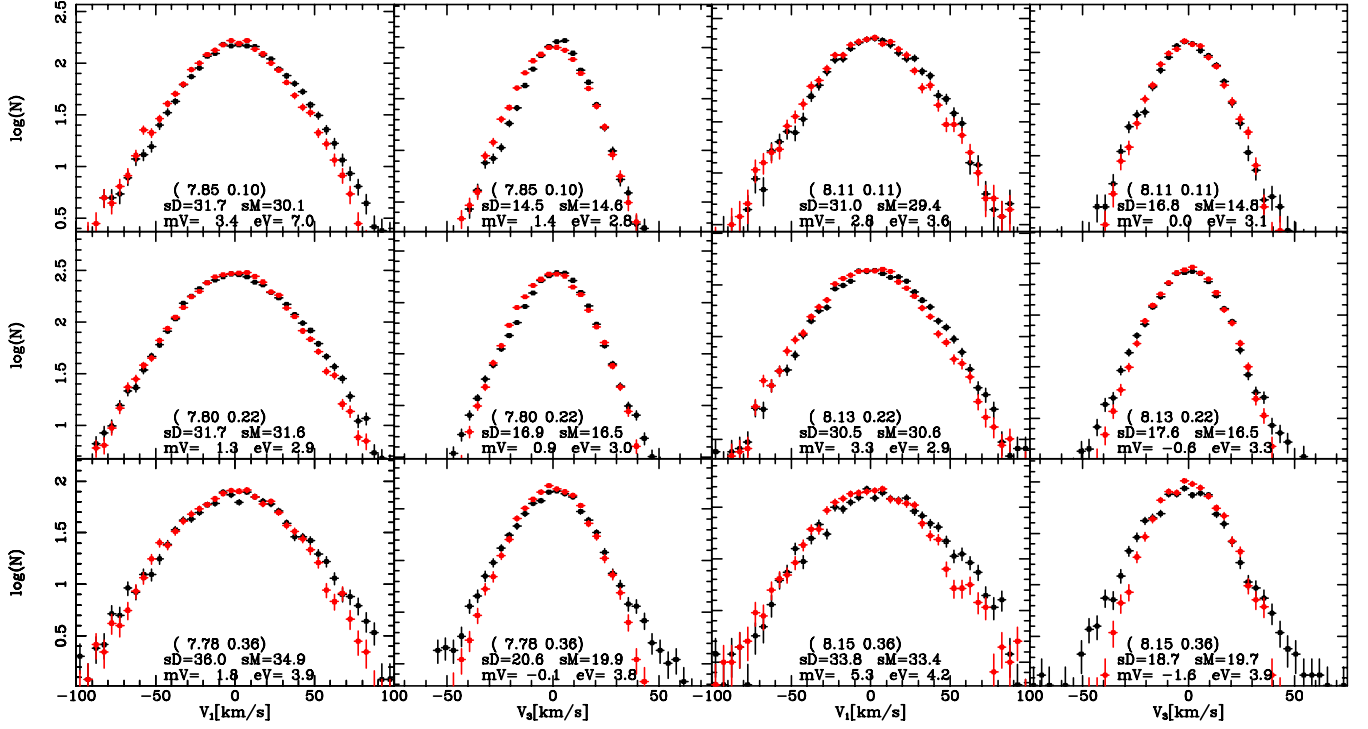
Figure 11. Distributions of $V_1 \simeq -v_r$ and $V_3 \simeq v_z$ for hot dwarfs. The black points show the RAVE data, red points the predictions of the B12 model when it is assumed that all hot dwarfs are younger than 5 Gyr and as such belong to the thin disc. At the lower middle of each panel are given the mean (R, z) coordinates of the bin; the standard deviation of the data after correction for error and the velocity dispersion at the mean coordinates of the Gaussian model described in Section 3; the mean of the data and the rms error of the velocities.
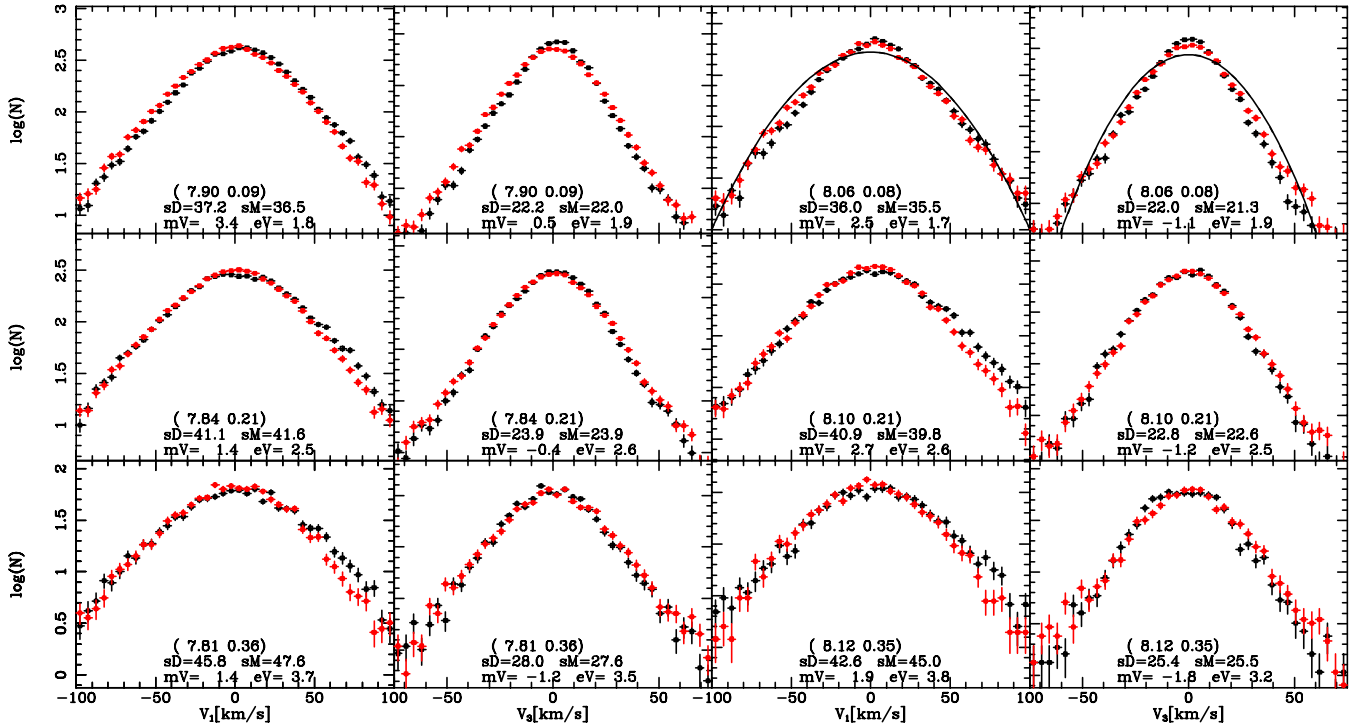
Figure 12. As Fig. 11, but for cool dwarfs. The red points now show the predictions of the B12 model when cool dwarfs are assumed to sample the entire DF. In the last two panels of the top row, we show the Gaussian distributions that were fitted in Section 3 to illustrate how well the dynamical model captures the deviations of the observed distribution from Gaussianity.
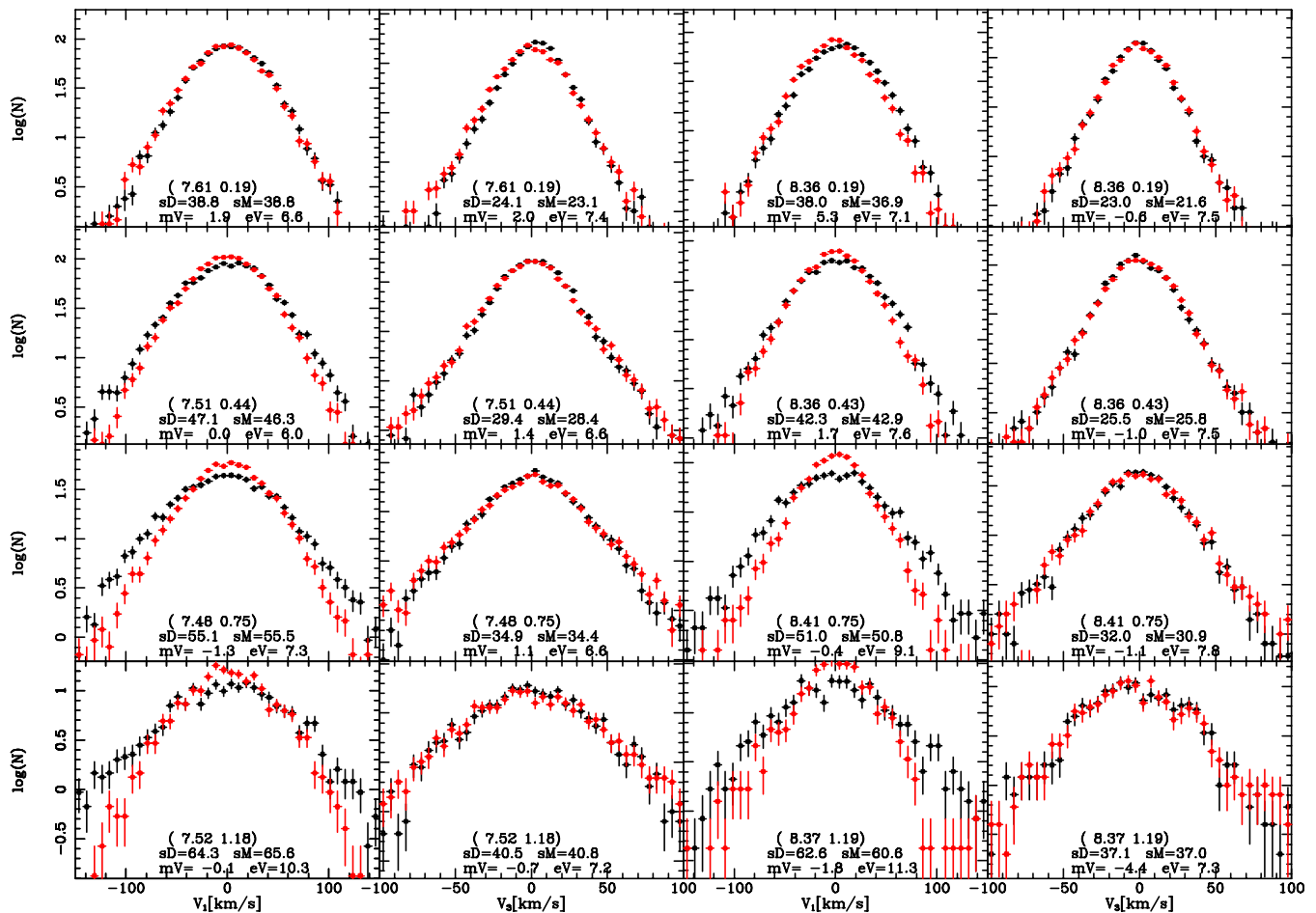
Figure 13. As Fig. 12, but for clump giants.

to overweight slightly the possibility that stars lie at the far ends of their distance PDFs (Sanders & Binney in preparation). We believe the impact of this effect to be small, so our model histograms correctly represent the model's predictions for a survey with the selection function and errors of RAVE.

We assume that the hot dwarfs are all younger than 5 Gyr (e.g. fig. 2 of Zwitter et al. 2010) and correspondingly restrict the B12 DF of these objects to the portion of the thin disc that is younger than 5 Gyr. The distributions of clump and non-clump giants and cool dwarfs are (rather arbitrarily) assumed to sample the whole DF.

5.1 Azimuthal velocities distributions

The red points in Figs 4–7 show the model's predictions for the v_ϕ components. Figs 4 and 5 show that the velocities of the clump giants are very similar to those of the non-clump giants. This result is in line with expectations, but serves to increase our confidence in our distance estimates for, as we shall see in Section 5.3, systematic errors in the distances of whole groups of stars distort the derived velocity distributions. Hence, consistency between the histograms for clump and non-clump giants suggests that our distances to non-clump giants, which are the hardest to determine, are no more in error than are the distances to clump giants.

In Figs 4 and 5, the models definitely underpopulate the wing at $v_\phi > \Theta_0$, especially away from the plane. This is likely to reflect the model's thick disc being radially too cool, as discussed below.

A notable difference between the observed and predicted distributions for both the giants and the hot dwarfs (Figs 4–6) is that at $R < R_0$ and $|z| \sim 0.5$ kpc, the black, measured, distribution is shifted to larger values of v_ϕ than the red predicted one. In the case of the hot dwarfs, a similar but distinctly smaller shift is seen at $R > R_0$. The smaller shift at $R > R_0$ is clearly connected to the fact that in Fig. 9 the $\langle v_\phi \rangle$ points for $R > R_0$ lie below those for $R < R_0$. At $z < 0.5$ kpc, the same phenomenon is evident for giants in Fig. 8. One possible explanation is that the Galaxy's circular-speed curve is falling with R relative to that of the model.

While the theoretical distribution depends only on the model's value 220 km s^{-1} for the local circular speed Θ_0, the observed velocities have been derived using both Θ_0 and a value $V_0 = 12.24$ km s^{-1} from Schönrich et al. (2010) for the amount by which the Sun's v_ϕ exceeds Θ_0. Hence, an offset between the red and black curves in Figs 4–7 can be changed by changing the assumed value of V_0: reducing V_0 shifts the black distribution to the left. However, the case for such a change is less than unconvincing because the shift is clear only at $R < R_0$ and $|z| \lesssim 0.5$ kpc. Moreover, in Fig. 7, for the cool dwarfs the model histograms provide excellent fits to the data. In Fig. 6, for the hot dwarfs the offset between the red and black histograms vanishes at $R > R_0$ near the plane but grows with $|z|$.

A more convincing case can be made for an increase in the width of the theoretical distributions of giants away from the plane.
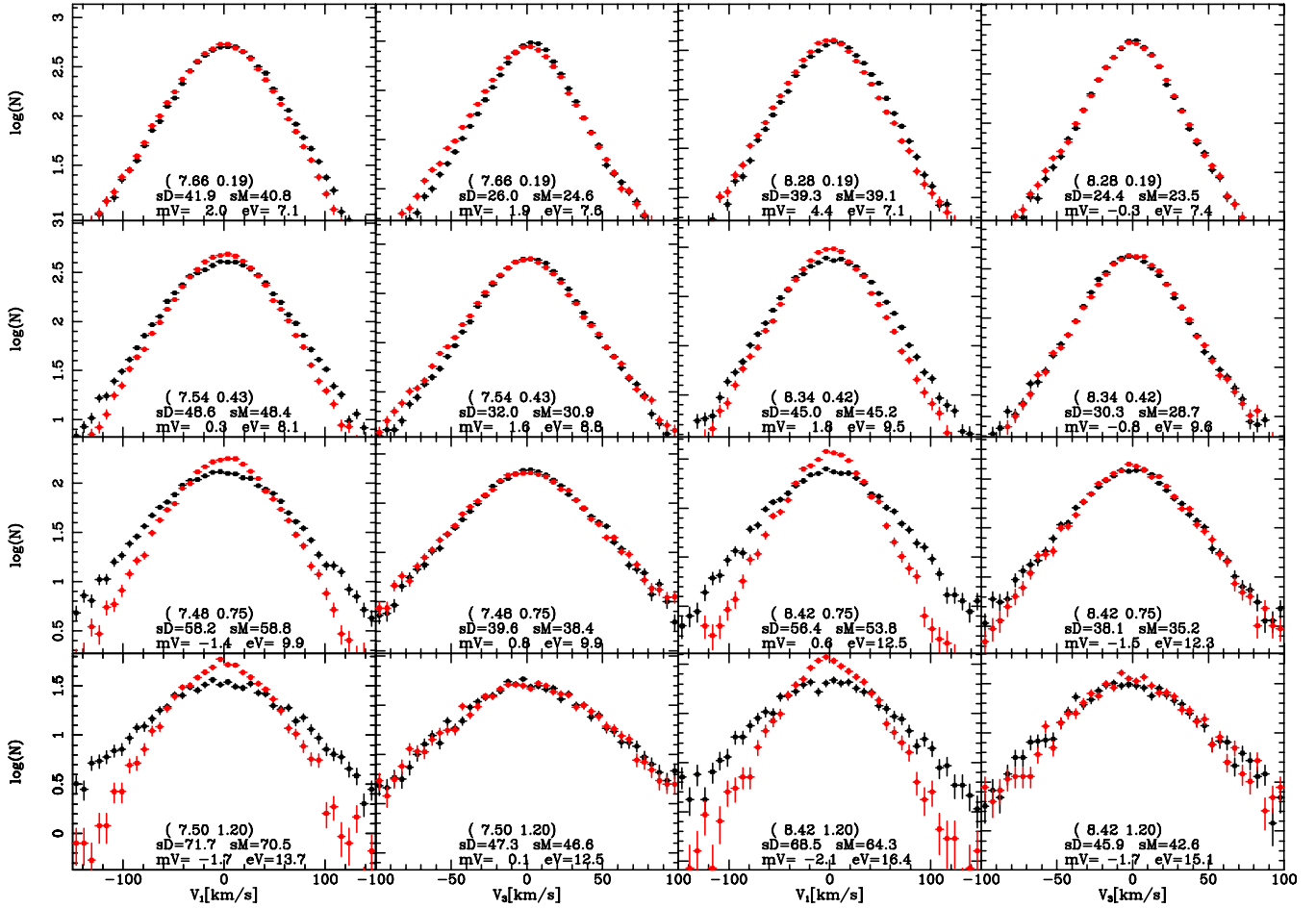
Figure 14. As Fig. 12, but for non-clump giants.

In addition to a possibly incorrect value of V_0, there are four other obvious sources of offsets between the observational and theoretical distributions of v_ϕ.

(i) Spiral arms must generate fluctuations in the mean azimuthal velocity of stars. Judging by oscillations with Galactic longitude in the observed terminal velocity of interstellar gas (e.g. Malhotra 1995) in a population such as hot dwarfs that have a low velocity dispersion. Moreover, it is now widely accepted that the irregular distribution of *Hipparcos* stars in the (U, V) plane of velocities (Dehnen 1998) is in large part caused by spiral arms perturbing the orbits of stars (De Simone, Wu & Tremaine 2004; Antoja et al. 2011; Siebert et al. 2012; McMillan 2013). The large (up to $20°$) value of the vertex deviation for hot dwarfs is surely also due to spiral structure. Spiral-induced modulations in $\langle v_\phi \rangle$ will vary quite rapidly with radius and thus could make significantly different contributions to $\langle v_\phi \rangle$ in our bins at $R < R_0$ and $R > R_0$.

(ii) The mean age of the stellar population is expected to decrease with increasing Galactocentric distance. Such a decrease would introduce a bias into a sample selected to be young such that there were more stars seen near pericentre than near apocentre than in a sample of older stars, so stars in the younger sample would tend to have larger values of v_ϕ than stars in the older sample. This effect could explain why the histograms for hot dwarfs show larger offsets than do those for cool dwarfs.

(iii) We are probably using a value of R_0 that is too small by ~ 3 per cent. Changing the adopted value of R_0 changes the supposed direction of the tangential vector $\boldsymbol{e}_\phi(\star)$ at the location of a star and thus changes the component of a star's Galactocentric velocity $\boldsymbol{v}$ that we deem to be v_ϕ. The velocity $\boldsymbol{v}$ is made up of the star's heliocentric velocity $\boldsymbol{v}_h$ and the Sun's largely tangential velocity $\boldsymbol{v}_\odot = \Theta_0 \boldsymbol{e}_\phi(\odot) + (U_0, V_0, W_0)$. For a star at a given distance, increasing R_0 diminishes the angle between $\boldsymbol{e}(\star)$ and $\boldsymbol{e}(\odot)$, and thus, by diminishing the angle between $\boldsymbol{e}_\phi(\star)$ and $\boldsymbol{v}_\odot$, tends to increase v_ϕ. Consequently, in Figs 4–7, increasing R_0 moves the black points to the right, away from the model's predictions.

(iv) We are probably using a value of Θ_0 that is too small by ~ 9 per cent. Increasing Θ_0 by $\delta\Theta$ simply moves the observational histogram to the right by $\delta\Theta$. However, since the asymmetric drift v_a of a population that has radial velocity dispersion σ_r scales as σ_r^2/Θ_0, increasing Θ_0 moves the theoretical histogram to the right by

$$\delta\Theta - \delta v_a = \left(1 + \frac{\sigma_r^2}{\Theta_0^2}\right)\delta\Theta, \tag{9}$$

so this upward revision will reduce by $(\sigma_r/\Theta_0)^2 \delta\Theta \sim 0.04\delta\Theta_0$ the offsets we obtained with our traditional choices of R_0 and Θ_0.

5.2 Velocities in the meridional plane

Figs 11–14 are the analogues of Figs 4–7 for components of velocity V_1 and V_3 (equation 2) in the meridional plane: black points

show observational histograms and red ones the predictions of the B12 model. V_1 is the component of velocity along the longest principal axis of the velocity ellipsoid at the star's location according to the Gaussian model fitted in Section 3. The sign convention is such that at the Sun $V_1 \simeq U = -v_R$. $V_3 \simeq W = v_z$ is the perpendicular velocity component. The left two columns are for bins with $R < R_0$, while the right two columns are for bins with $R > R_0$. At the lower middle of each panel are given the mean (R, z) coordinates of stars in the bin; the standard deviation of the data after correction for error (sD) and the velocity dispersion at the mean coordinates of the Gaussian-model described in Section 3 (sM); the mean of the data (mV) and the rms error of the velocities (eV).

All distributions are significantly non-Gaussian (i.e. the distributions are far from parabolic) and the B12 model captures this aspect of the data beautifully. The last two panels in the top row of Fig. 12 illustrate this phenomenon by showing the parabolas of the Gaussian distributions fitted in Section 3. Notwithstanding the non-Gaussian nature of the velocity distributions, in every bin there is good agreement between the standard deviation of the data sD and the dispersion at of the Gaussian model sM at the barycentre of the bin. This result implies that equations (4) can be safely used to recover the principal velocity dispersions throughout the studied region.

The model is particularly successful in predicting the V_3 distributions of both dwarfs and giants. In the case of the dwarfs, the only blemish on its V_3 distributions is a marginal tendency for the distribution of hot dwarfs to be too narrow at high $|z|$.

The principal differences between the model and observed V_1 distributions of dwarfs arise from left–right asymmetries in the data. For example, in the third panels from the left in the first and second rows of Fig. 11 for hot dwarfs, the black points lie systematically above the red points for $V_1 > 0$ (inward motion), a phenomenon also evident in the top-left panel of that figure. In the first and third panels in the second row of Fig. 12 for cool dwarfs, a similar phenomenon is evident in that the red points lie above the black points at $V_1 < 0$. A contribution to these divergences must come from star streams, which Dehnen (1998) showed to be prominent in the local *UV* plane.

Figs 13 and 14 for clump and non-clump giants show V_1 and V_3 distributions in bins that extend to much further from the plane. In both cases, the model and observed V_3 distributions agree to within the errors. Given the smallness of the error bars in the case of the giants and the fact that the data extend to a distance from the plane that is more than 10 times the extent of the GCS data to which the B12 model was fitted, the agreement between the observed and theoretical V_3 histograms in Fig. 14 amounts to a very strong endorsement of the B12 model.

The observed V_1 distributions for clump and non-clump giants are consistent with one another, and the superior statistics of non-clump giants highlight the deviations from the model predictions. Near the plane, the model fits the data well, but the further one moves from the plane, the more clear it becomes that the model distribution of V_1 is too narrow. This phenomenon arises because in B12, contrary to expectation, the thick disc needed to be radially cooler than the thin disc. The RAVE data are indicating that this was a mistake. In B12, two factors shared responsibility for the radial coolness of the thick disc. One was the ability of the thin-disc DF to fit the wings of the U and V distributions in the GCS, leaving little room for the thick disc's contribution there. The other factor was an indication from SDSS that $\langle v_\phi \rangle$ does not fall rapidly with distance from the plane. Fig. 5 relates to this second point, and indeed the RAVE data show more stars with large v_ϕ than the model, especially at large

$|z|$. In B12, it was demonstrated that there is a clean dynamical trade-off between $\langle v_\phi \rangle$ and σ_ϕ in the sense that an increase in the former has to be compensated by a decrease in the latter. Moreover, σ_ϕ is dynamically coupled to $\langle V_1^2 \rangle^{1/2}$, so if one is reduced, the other must be reduced as well. Hence, large $\langle v_\phi \rangle$ implies small $\langle V_1^2 \rangle^{1/2}$. There is a puzzle here that requires further work.

5.3 Effect of distance errors

Our model predictions already include the effects of random distance (and velocity) errors. Now, we investigate how *systematic* errors in our spectrophotometric distances affect the derived kinematics. This investigation is motivated in part by the indication in Binney et al. (2013) from the kinematic test of Schönrich, Binney & Asplund (2012) that distances to giants might be overestimated by as much as 20 per cent, and distances to the hottest dwarfs underestimated by a similar amount.

The black points in Fig. 15 are identical to those in the corresponding panels of Fig. 14, but the red model points have been modified by adding $-5\log_{10}(e) \times 0.2$ to the randomly chosen distance modulus of each star before evaluating the DF. This modification enables us to model the impact on the survey of catalogued distances being on average 20 per cent too large.

The figure shows that such distance errors introduce left–right asymmetry into the model distributions of both V_1 and V_3 similar to that evident in the V_1 distribution of hot dwarfs. The red values of mV at the bottom middle of each panel, show the mean values of V_1 and V_3 for the model histograms. We see that these values are non-zero and of comparable magnitude to the mean values of the observed histograms given in Fig. 14. Thus, non-zero mean values of $\langle V_1 \rangle$ and $\langle V_3 \rangle$ may arise from distance errors rather than from real streaming motion. However, near the plane our distance errors induce negative mean values of V_1 (net outward motion), whereas the data histogram shows a smaller positive mean value of V_1.

Physically, overestimating distances makes the V_1 distribution skew to positive V_1 because the survey volume is not symmetric in Galactic longitude, and at certain Galactic longitudes, proper motion generated by the disc's differential rotational is wrongly interpreted to be proper motion associated with motion towards the Galactic Centre.

The assumption that distances are overestimated also broadens the model distribution of V_1 far from the plane, with the result that, for example, in the third row of Fig. 15 the red and black points for V_1 lie significantly closer than in the corresponding panels of Fig. 14.

Fig. 16 is the analogue of Fig. 5 for the case in which the distances to giants have been overestimated by 20 per cent. In the top-left panel, for small $|z|$ and $R < R_0$, the agreement between model and data is now less good than it is in Fig. 5, but in every other panel, the agreement is at least as good as in Fig. 5 and for $R > R_0$ it is distinctly improved. Thus, the v_ϕ distributions by no means speak against the suggestion that many distances have been overestimated by ~20 per cent.

While in Fig. 15 distance errors have improved the fit to the data only at $|z| > 0.5$ kpc and weakened the fit closer to the plane, it is perfectly possible that systematic errors are largely confined to more distant stars and/or ones further from the plane. In fact, such an effect is inevitable even if the errors in distances of individual stars were inherently unbiased because stars that happen to pick up a positive distance error will tend to accumulate in the distant bins, and conversely for stars that happen to pick up a negative distance error. When we modified the model's predictions to allow
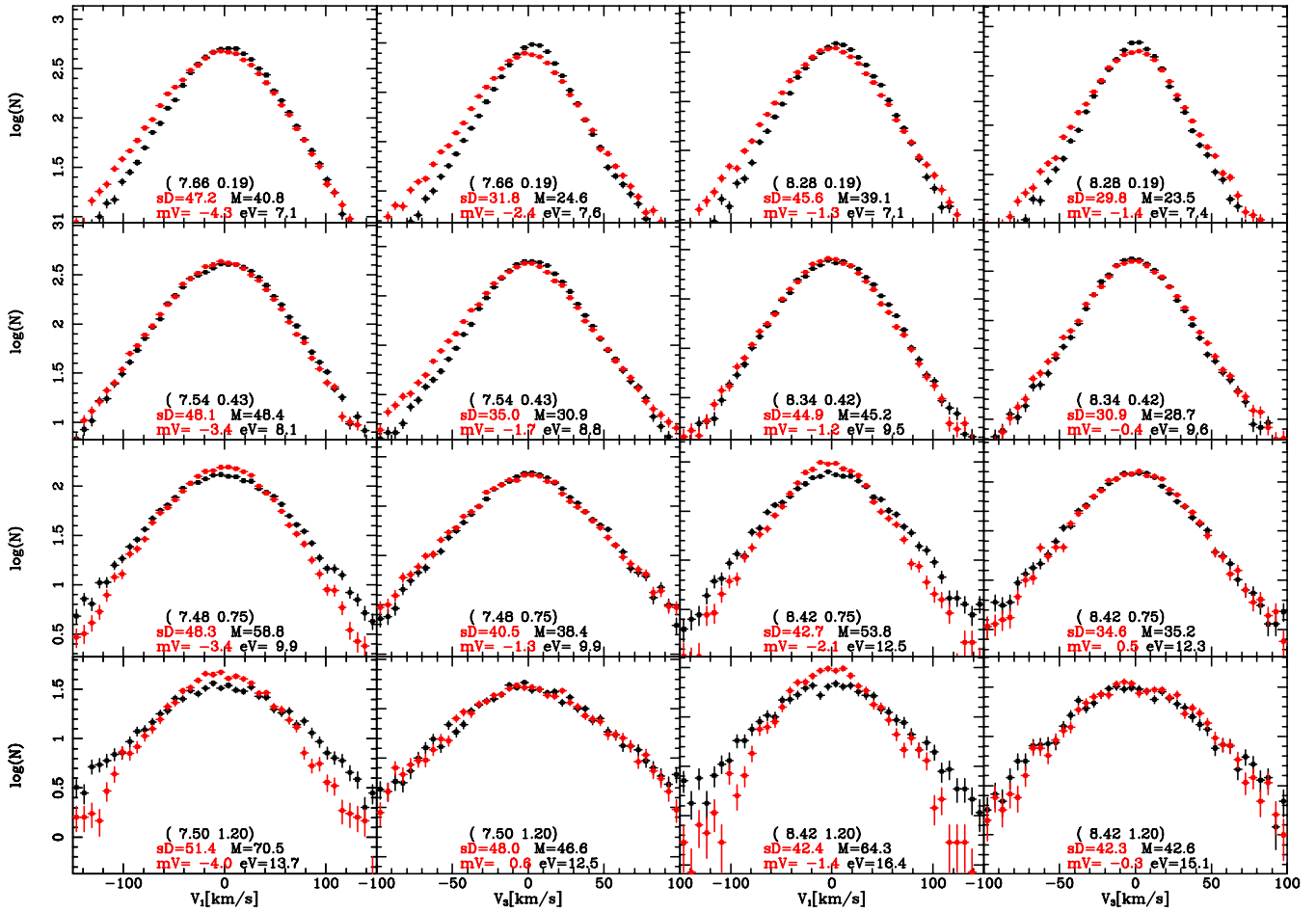
Figure 15. The black points are identical to those plotted in Fig. 14. The red model histograms have been modified by supposing that the catalogued distance to each (giant) star is 20 per cent larger than it should be. The values sD and mV given at the bottom are now the standard deviation and mean of the red histogram.
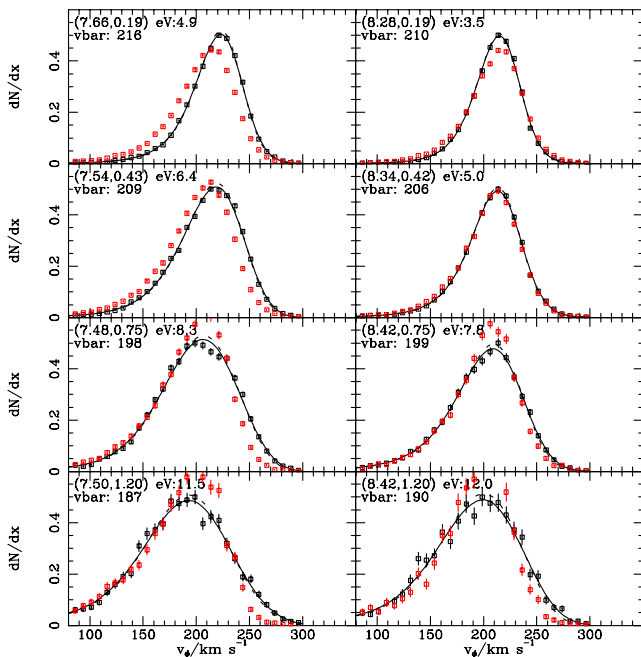
Figure 16. As Fig. 5, but when the adopted distances to these (giant) stars are 20 per cent larger than they should be.

for random distance errors, we did not capture this effect because the spatial bin to which a star is then assigned is not affected by whether it is supposed to have had its distance over- or underestimated.

6 DISCUSSION

Siebert et al. (2011) reported a significant radial gradient in the mean $\langle v_R \rangle$ of velocities of stars reduced by the RAVE VDR2 pipeline. Williams et al. (2013; hereafter W13) used data from the VDR3 pipeline to analyse the mean velocity field $\langle v \rangle$ of clump stars. In a steady-state, axisymmetric Galaxy, the only non-vanishing component of this field would be $\langle v_\phi \rangle$ and it would have a maximum in the plane, falling away with $|z|$ symmetrically on each side. Instead fig. 11 of W13 indicates that the velocity field of the clump stars has both $\langle v_R \rangle$ and $\langle v_z \rangle$ components non-zero and with gradients in both the R and z directions, and there is a lack of symmetry about the plane. W13 strike a cautionary note by showing that the $\langle v_R \rangle$ and $\langle v_z \rangle$ components are sensitive to which proper motions one adopts, but they demonstrate that $\langle v \rangle$ is insensitive to the adopted absolute magnitude of clump stars.

As W13 show, probing the observed velocity field is made difficult by the complexity of the three-dimensional volume surveyed by RAVE: samples assembled to have a progression of values of one coordinate inevitably differ systematically in another coordinate as well. For this reason, it is crucial to compare observational results

with the predictions of a model that suffers the same selection effects. W13 compare the observations to mock catalogues selected by the code GALAXIA (Sharma et al. 2010) from the Besançon model (Robin et al. 2003). Our comparisons differ in that (i) we have used a fully dynamical model, based on Jeans' theorem, rather than the essentially kinematic Besançon model and (ii) we assign new velocities to existing stars rather than drawing an entirely new sample from the model – this procedure has the great advantage that we do not have to engage with the survey's complex photometric selection function.

Our emphasis has been different in that we have focused on entire velocity distributions rather than just the distributions' means. This has been possible because we have a more prescriptive dynamical model, but it has resulted in our using much bigger bins than W13. In particular, we have grouped together stars above and below the plane, which will inevitably wash out some of the structure in the (R, z) plane seen by W13.

Our demonstration that introducing plausible systematic errors in the assumed distances to stars causes the model histograms to acquire mean velocities that are similar in magnitude to those found by W13 must be a concern even though the particular systematic in distance error that we have considered does not generate the observed pattern of mean velocities. The extent to which distance errors broaden the distributions of V_1 is surprising and interesting given the difficulties one encounters finding a dynamical model that is consistent with all the data for $\langle v_\phi \rangle$ and $\langle V_1^2 \rangle^{1/2}$ in the absence of systematic distance errors.

7 CONCLUSIONS

We have analysed the kinematics of ∼400 000 RAVE stars for which Binney et al. (2013) have deduced PDFs in distance modulus. The sample divides naturally into clump and non-clump giants, hot and cool dwarfs. For each of these classes, and without binning the data, we have obtained analytic formulae for the structure of the velocity ellipsoid at each point in the (R, z) plane. We are able to map the velocity ellipsoid of the giants to distances ∼2 kpc from the Sun and find that at (R, z) the direction of the longest axis is inclined to the Galactic plane by an angle ∼0.8 arctan(z/R). The lengths of the (R, z) semi-axes are in the ratio $\sigma_3/\sigma_1 \simeq 0.6$. The velocity dispersions rise with distance from the plane, from $\sigma_r \simeq 37 \text{ km s}^{-1}$, $\sigma_z \simeq 21 \text{ km s}^{-1}$ at $(R_0, 0)$ to $\sigma_r \simeq 82 \text{ km s}^{-1}$, $\sigma_z \simeq 54 \text{ km s}^{-1}$ at $(R_0, 2 \text{ kpc})$. The velocity ellipsoid of the cool dwarfs cannot be traced to great distances, but it is consistent with being the same as that of the giants. In the plane, the velocity dispersions of the hot dwarfs are $\sigma_r \simeq 29 \text{ km s}^{-1}$ and $\sigma_z \simeq 14 \text{ km s}^{-1}$ and they increase rather slowly with distance from the plane. From equations (3) and (4) and Table 2, one can compute for any of our four classes of stars the structure of the velocity ellipsoid at a general point in the (R, z) plane.

We have used a novel formula to obtain remarkably precise analytic fits to the distinctly non-Gaussian v_ϕ distributions for eight bins in the (R, z) plane. The complete v_ϕ distributions at these points can be recovered for any of the four classes of stars by inserting values from either Table 3 or Table 4 into equations (7) and (8).

We have compared our observational velocity histograms with the predictions of a dynamical model that was fitted to the local velocity distribution and the Gilmore & Reid (1983) vertical density profile. When making this comparison, we assume only that the survey's selection function is velocity blind (which it certainly is) and we are able to model the effects of errors in both distances and velocities with considerable completeness.

Overall, the agreement between the model's predictions and the data is remarkably good and offers strong support for the assumptions on which the dynamical model rests, including its gravitational potential. There is, however, a tendency for the distribution of observed v_ϕ components to be shifted to larger values than the model predicts. A possible contributory factor to this offset may be overestimation of the Sun's peculiar V velocity, but the offset can be generated in several ways, including spiral arms, the age gradient within the disc and use of incorrect values of R_0 and Θ_0.

The dynamical model performs outstandingly well in predicting the distributions of vertical velocity components V_3 of all star classes. These distributions are considerably more sharply peaked than Gaussians and the model captures this phenomenon beautifully. At $|z| < 0.5$ kpc, the model predicts the distributions of radial components V_1 nearly as successfully, but at greater distances from the plane the model predicts distributions of V_1 that are too narrow. This problem is undoubtedly connected to the surprising conclusion of B12 that the thick disc is radially cooler than the thin disc, a conclusion driven by both the structure of the GCS histograms for U and the strong mean rotation of SDSS stars far from the plane. The RAVE data also require that at $|z| > 1$ kpc there are unexpectedly many stars at large v_ϕ, and this fact constraints our ability to make the thick disc radially hotter as the V_1 histograms imply.

One way to resolve, or at least ameliorate, the problem is to suppose that stars in the most distant bins have had their distances overestimated by ∼20 per cent. Similar distance overestimates in the nearer bins would impair the nice agreement between theory and observation. However, it is inevitable that stars placed in the most distant bins have, on average, overestimated distances, so it is plausible that distance overestimates contribute significantly to the anomalies in the high-$|z|$ bins.

This study clearly indicates that the approach to Galaxy modelling developed in B12 is well worth developing. There are several directions in which to go. First, a new DF of the current type should be fitted to the richer body of observational data that is now available using an updated Galactic potential Φ. Next, this DF and these data should be used as a starting point for a redetermination of Φ along the lines outlined by McMillan & Binney (2013). Currently, the DF is being extended to include chemistry alongside age (Binney & Sanders 2013): this extension should markedly increase our ability to diagnose Φ because the requirement that several stellar populations that differ in both their chemistry and their kinematics exist harmoniously in a common potential will strongly constrain Φ.

REFERENCES

Antoja T., Figueras F., Romero-Gómez M., Pichardo B., Valenzuela O., Moreno E., 2011, MNRAS, 418, 1423

Binney J., 2012, MNRAS, 426, 1328 (B12)

Binney J., Sanders J. L., 2013, in Feltzing S., Zhao G., Walton N. A., Whitelock P. A., eds, Proc. IAU Symp. 298, Setting the scene for Gaia and LAMOST. Cambridge Univ. Press, Cambridge

Binney J. et al., 2013, MNRAS, 437, 351

Burnett B., 2010, DPhil thesis, Oxford University

Burnett B. et al., 2011, A&A, 532, 113

De Simone R., Wu X., Tremaine S., 2004, MNRAS, 350, 627

Dehnen W., 1998, AJ, 115, 2384

Dehnen W., Binney J., 1998, MNRAS, 298, 387

Eisenstein D. et al., 2011, AJ, 142, 72

Gilmore G., Reid N., 1983, MNRAS, 202, 1025

Holmberg J., Nordström B., Andersen J., 2007, A&A, 475, 519

Kordopatis G. et al., 2013, AJ, 146, 134

Malhotra S., 1995, ApJ, 448, 138

McMillan P. J., 2011, MNRAS, 414, 2446

McMillan P. J., 2013, MNRAS, 430, 3276

McMillan P. J., Binney J., 2013, MNRAS, 433, 1411

Press W. H., Teukolsky S. A., Vetterling W. T., Flannery B. P., 1994, Numerical Recipes in C. Cambridge Univ. Press, Cambridge

Robin A., Reylé C., Derrière S., Picaud S., 2003, A&A, 409, 523

Röser S., Schilbach E., Schwan H., Kharchenko N. V., Piskunov A. E., Scholz R.-D., 2008, A&A, 488, 401

Schönrich R., Binney J., Dehnen W., 2010, MNRAS, 403, 1829

Schönrich R., Binney J., Asplund M., 2012, MNRAS, 420, 1281

Sharma S., Bland-Hawthorn J., Johnston R., Binney J. J., 2010, ApJ, 370, 3

Siebert A. et al., 2008, MNRAS, 391, 793

Siebert A. et al., 2011, MNRAS, 412, 2026

Siebert A. et al., 2012, MNRAS, 425, 2335

Steinmetz M. et al., 2006, AJ, 132, 1645

van der Kruit P. C., Searle L., 1981, A&A, 95, 105

Williams M. et al., 2013, MNRAS, 436, 101 (W13)

Yanny B. et al., 2009, AJ, 137, 4377

York D. G. et al., 2000, AJ, 120, 1579

Zacharias N., Finch C., Girard T., Henden A., Bartlett J., Monet D., Zacharias M., 2013, AJ, 145, 44

Zwitter T. et al., 2010, A&A, 522, A54

This paper has been typeset from a TEX/LATEX file prepared by the author.